Elucidating the pivotal role of TSPO in porphyrin-related cellular processes, in Bacillus cereus

Catherine Duport, Jean Armengaud, Caroline Schmitt, Didier Morin, Jean-Jacques Lacapère

Biochimie xxx (xxxx) xxx

Contents lists available at ScienceDirect

Biochimie

journal homepage: www.elsevier.com/locate/biochi

Elucidating the pivotal role of TSPO in porphyrin-related cellular processes, in *Bacillus cereus*

Catherine Duport [a, *], Jean Armengaud [b], Caroline Schmitt [c, d], Didier Morin [e], Jean-Jacques Lacapère [f]

[a] Avignon Université, INRAE, UMR SQPOV, F-84914, Avignon, France
[b] Université Paris Saclay, CEA, INRAE, Département Médicaments et Technologies pour la Santé (DMTS), SPI, 30200, Bagnols-sur-Cèze, France
[c] Assistance Publique Hôpitaux de Paris (AP-HP), Centre Français des Porphyries, Hôpital Louis Mourier, 92700, Colombes, France
[d] INSERM U1149, Center for Research on Inflammation (CRI), Université de Paris, 75018, Paris, France
[e] INSERM, U955, équipe 3, Faculté de Médecine, Université Paris Est, 94010, Creteil, France
[f] Sorbonne Université, Ecole Normale Supérieure, PSL University, CNRS UMR 7203, Laboratoire des BioMolécules (LBM), 4 place Jussieu, F-75005, Paris, France

ARTICLE INFO

Article history:
Received 11 January 2024
Received in revised form
19 February 2024
Accepted 21 February 2024
Available online xxx

Handling Editor: Dr B Friguet

Keywords:
TSPO
Porphyrins
Gram-positive bacteria
Tryptophan
Energy metabolism

ABSTRACT

A structural homolog of the mammalian TSPO has been identified in the human pathogen *Bacillus cereus*. BcTSPO, in its recombinant form, has previously been shown to bind and degrade porphyrins. In this study, we generated a Δ*tspO* mutant strain in *B. cereus* ATCC 14579 and assessed the impact of the absence of BcTSPO on cellular proteomics and physiological characteristics. The proteomic analysis revealed correlations between the lack of BcTSPO and the observed growth defects, increased oxygen consumption, ATP deficiency, heightened tryptophan catabolism, reduced motility, and impaired biofilm formation in the Δ*tspO* mutant strain. Our results also suggested that BcTSPO plays a crucial role in regulating intracellular levels of metabolites from the coproporphyrin-dependent branch of the heme biosynthetic pathway. This regulation potentially underlies alterations in the metabolic landscape, emphasizing the pivotal role of BcTSPO in *B. cereus* aerobic metabolism. Notably, our study unveils, for the first time, the involvement of TSPO in tryptophan metabolism. These findings underscore the multifaceted role of TSPO, not only in metabolic pathways but also potentially in the microorganism's virulence mechanisms.

1. Introduction

The Translocator proteins (TSPO), originally known as the Peripheral Benzodiazepine Receptors (PBR) [1], are conserved transmembrane proteins characterized by five alpha-helical regions [1,2]. They are found in organisms ranging from bacteria to humans [2,3]. In humans, two isoforms of TSPO have been identified: TSPO1 and TSPO2. TSPO1, primarily localized in the outer mitochondrial membrane, is widely expressed in various tissues, and is implicated in a diverse array of cellular processes, including cell proliferation, differentiation, apoptosis, immunomodulation, tetrapyrrole metabolism, oxidative stress response, steroid biosynthesis, and mitochondrial physiology [4]. In contrast to TSPO1, TSPO2 exhibits erythroid-specific expression and is localized in the endoplasmic reticulum, nucleus, and plasma membranes [5]. Bacterial TSPOs, also known as tryptophan-rich sensory protein/translocator protein, share approximately 25–35% sequence identity with TSPO1 [6]. The first bacterial protein homologous to TSPO1, known as RsTSPO, was discovered in the photosynthetic purple bacterium *Rhodobacter sphaeroides* [6]. In this Gram-negative bacterium, RsTSPO is located in the outer membrane and regulates the expression of genes encoding enzymes of the photosynthetic pigment biosynthetic pathway in response to oxygen levels [7]. RsTSPO was also involved in the efflux of porphyrins [8]. In *Sinorhizobium melitoli*, a legume symbiont bacterium, TSPO regulates the expression of the nutrient deprivation-induced (*ndi*) locus in response to nutrient deficiency or anaerobic conditions and contributes to porphyrin transport [9]. In the soil bacterium *Pseudomonas fluorescens*, TSPO was shown to be involved in envelope stress response [10]. *Fremyella diplosiphon*, an oxygenic

* Corresponding author.
E-mail address: catherine.duport@univ-avignon.fr (C. Duport).

https://doi.org/10.1016/j.biochi.2024.02.008

Abbreviations

BcTSPO	*Bacillus cereus* translocator protein
CPD	CoproPorphyrin-Dependent
COG	Cluster of Orthologous Groups
DAP	Differentially Accumulated Protein
GO	Gene Ontology
KEGG	Kyoto Encyclopedia of Genes and Genomes
LB	Lysogeny broth
MS	Mass spectrometry
NSAF	Normalized Spectral Abundance Factor
ORF	Open Reading Frame
PPIX	Protoporphyrin IX
ROS	Reactive Oxygen Species
TCA	Tricarboxylic acid cycle

photosynthetic cyanobacterium, synthesizes three TSPO proteins involved in responses to various abiotic stresses, including oxidative, osmotic, and nutrient stress. It has been proposed that these proteins may regulate intracellular levels of tetrapyrroles, thereby influencing the metabolic pathways controlled by these molecules [11].

Despite extensive research on TSPO in eukaryotes and other bacterial species, its role within the *Bacillus cereus* group remains remarkably underexplored. The *Bacillus cereus* group includes at least twelve closely related Gram positive bacteria species with various ecological niches and pathogenic properties [12,13]. *B. cereus* (*sensu stricto*) is one of the most studied members of the *B. cereus* group. *B. cereus* is an endospore-forming, anaerobic facultative, motile bacterium, renowned for its adaptability to a wide range of environments, as well as its capacity to cause food-borne illnesses and infections in humans [14,15]. Despite its clinical significance, the molecular determinants governing *B. cereus*' virulence, stress responses, and survival strategies remain only partially understood.

The type strain of *B. cereus* is the strain ATCC 14579 [16], which synthesizes a 17.835 kDa TSPO protein, known as BcTSPO. When produced in *Escherichia coli* BcTSPO can catalyze the degradation of protoporphyrin IX (PPIX) on the presence of oxygen and exposure to light [17,18]. Since this degradation results in a significant reduction in the production of Reactive Oxygen Species (ROS) generated from the photo-oxidation of PPIX, it was proposed that BcTSPO could promote ROS neutralization, and thus contribute to oxidative stress response [17].

The present study aims to bridge the existing knowledge gap between *in vitro* and *in vivo* experiments by investigating the role of BcTSPO, in *B. cereus* ATCC 14579. By employing a multidisciplinary approach encompassing proteomics, biochemical analyses, and functional assays, we seek to elucidate the functions of BcTSPO within the context of this bacterium. Through this investigation, we aim to shed light on how BcTSPO contributes to major metabolic functions, and potential virulence of *B. cereus*.

2. Material and methods

2.1. Bacterial strains, mutant construction and complementation

The model strain used in this study is *B. cereus* ATCC 14579 [16]. The Δ*tspO* mutant was generated by allelic replacement, using the temperature-sensitive pMAD plasmid [17]. Briefly, 1-kbp flanking DNA sequences upstream and downstream of the BC_3136 open reading frame (ORF) were amplified using the appropriate oligonucleotide primers (Table S1). The up- and downstream fragments were fused using the primer-incorporated restriction sites, and cloned into pCR-TOPO 2.1 plasmid (Invitrogen). The resulting plasmid was digested with *Stu*I and ligated with a *Sma*I-digested spectinomycin fragment. The new plasmid was digested with *Eco*RI and *Sal*I, and the resulting fragment was cloned into pMAD digested by the same enzymes. The recombinant plasmid was used to transform *B. cereus* ATCC 14579 cells, by electroporation. Mutant allele was confirmed by PCR with oligonucleotide primers located upstream and downstream of the DNA regions used for homologous recombination. For complementation assays, the *tspO* gene was PCR amplified from *B. cereus* ATCC 14579 using primers listed in Supplementary Table S1, and inserted into the pHT304 plasmid vector [17] using primer-incorporated restriction sites. The plasmid pHT304-*tspO* was introduced in *B. cereus* cells by electroporation.

2.2. Growth conditions and parameters

Wild-type (WT) *B. cereus* ATCC 14579 and the Δ*tspO* mutant strains were routinely grown in Lysogeny broth (LB) medium. For proteomic and phenotypic analyses, bacteria were aerobically cultivated in a chemically-defined MOD medium buffered at pH 7.2 [19] at 37 °C, without addition of mineral salts but with a 30 mM glucose supplement (MODG). Cultures were inoculated to an optical density at 600 nm (OD_{600}) of 0.02 from an overnight culture. Microplate titer cultures were performed using 200 µl of culture medium and a temperature-controlled, automated optical density reader (Flx-Xenius XMA, Safas, Monaco). Batch cultures were performed in 2 L flasks containing 500 mL MODG medium. For proteomic analyses, 100-mL were harvested at OD ~0.2. Cells and culture supernatants were separated by centrifugation at 10,000×*g* for 10 min at 4 °C. Cell pellets were immediately stored at −80 °C until analysis.

Growth of *B. cereus* WT and Δ*tspO* strains was monitored spectrophotometrically at 600 nm. The maximal specific growth rate (μ_{max}) was calculated using the modified Gompertz equation [20]. Concentrations of glucose, acetate, lactate, ethanol, formate, and succinate were quantified in filtered supernatants by employing enzymatic kits obtained from BioSenTec and Megazyme. The kits were utilized in accordance with the manufacturer's instructions.

2.3. Proteomics analysis

Protein and peptide samples from cell pellets were prepared according to previously established methods [21]. Peptides were separated using an Ultimate 3000 nano LC system coupled to a Q-Exactive HF mass spectrometer from Thermo Scientific for analysis. Peptide mixtures (10 µL) were loaded and desalted online on a reverse-phase Acclaim PepMap 100C18 precolumn (5 mm, 100 Å, 300 µm ID x 5 mm), and subsequently resolved based on their hydrophobicity on a nanoscale Acclaim Pepmap 100C18 column (3-µm bead size, 100 Å pore size, 75 µm ID x 500 mm) at a flow rate of 200 nL/min. This separation was achieved using a bi-modal gradient that combined buffer B (0.1% HCOOH, 80% CH_3CN, 20% H_2O) and buffer A (0.1% HCOOH, 100% H_2O).

Peptide digests of cellular proteins were eluted following a 90-min gradient (4–25% buffer B in 75 min, followed by 25–40% buffer B in 15 min), while extracellular proteins were eluted with a 60-min gradient (4–25% buffer B in 50 min, followed by 25–40% buffer B in 10 min). We used a Top-20 method, with full mass spectrometry (MS) scans acquired in the Orbitrap mass analyzer, covering an *m/z* range from 350 to 1500, with a resolution of 60,000. After each scan, the 20 most abundant precursor ions were

sequentially chosen for fragmentation and MS/MS acquisition at a resolution of 15,000. We employed a 10-sec dynamic exclusion window to improve the detection of low-abundance peptides. Only double- and triple-charged ions were selected for MS/MS analysis. Sequences were assigned using the Mascot Daemon search engine (version 2.5.1, Matrix Science) against the *B. cereus* ATCC 14579 Uniprot Database. Peptide mass tolerance and MS/MS fragment mass tolerance were set to 5 ppm and 0.02 Da, respectively. The search considered carbamidomethylation of cysteine residues as fixed modification, while oxidation of methionine (M) and deamidation of asparagine and glutamine (NQ) were included as variable modifications. All peptide matches with a peptide score associated with a Mascot *p*-value lower than 0.05 were retained. Proteins were considered valid when at least two distinct peptide sequences were detected in the same sample, resulting in a false discovery rate lower than 1% [22]. Changes in protein abundance between the wild-type (WT) and Δ*tspO* mutant were analyzed using the TFold test [23]. Significant changes were identified when the adjusted *p*-value was less than 0.05 and the |fold-change| was ≥1.5. The mass spectrometry proteomics data have been deposited in the ProteomeXchange Consortium via the PRIDE partner repository, with dataset identifier PXD048360.

2.4. Catalase activity assays

The catalase activity of whole cells was assessed spectrophotometrically by monitoring the rate of H_2O_2 decomposition at 240 nm and 25 °C. In summary, 1 mL of mid-exponential growth phase cultures with an OD_{600} of 0.2, including both WT and Δ*tspO* mutant strains, was pelleted via centrifugation at 1000×*g* for 10 min. Afterward, they were washed once with ice-cold phosphate-buffered saline (PBS) and resuspended in 500 μL of PBS. The reaction was initiated by adding 2 μL of 30% H_2O_2, and the reduction in absorbance was recorded every 30 min over a 4-h period. The amount of enzyme activity that decomposed 1 mol/mL of H_2O_2 per min was defined as 1 unit [24].

2.5. Detection of reactive oxygen species (ROS)

ROS production was assessed using the fluorescent dye 2′,7′-dichlorodihydrofluorescein diacetate (DCFH-DA; Sigma-Aldrich). Two milliliters of mid-exponential growth phase cultures with an OD_{600} of 0.2, comprising both WT and Δ*tspO* mutant strains, were pelleted via centrifugation at 1000×*g* for 10 min. After two washes with PBS, the cell pellets were resuspended in 500 μL of PBS. Subsequently, a 200-μl aliquot of each sample was transferred into a 96-well fluorescence microplate, and the samples were incubated with one μl of 10 mM DCFH-DA for 2 h at 37 °C. ROS production was quantified using the scanning unit (excitation λ = 485 nm, emission λ = 517 nm, Synergy HT multimode microplate reader). The background fluorescence of PBS and the autofluorescence of bacterial cells incubated without DCFH-DA were measured to calculate the net fluorescence emitted by bacteria.

2.6. ATP quantification

ATP levels were quantified using the BacTiter-Glo Microbial Cell Viability Assay (Promega), following the manufacturer's instructions. In each microplate well, 100 μl of exponentially growing WT and Δ*tspO* mutant cells were added. The bioluminescence reaction was triggered with the addition to each well of 100 μl of BacTiter-Glo™ reagent, prepared in accordance with the manufacturer's guidelines. Following thorough mixing, luminescence was measured using a Synergy HT Microplate Reader after a 10-min incubation at room temperature. Specific ATP levels were determined by dividing the luminescence values of each sample by the corresponding OD_{600nm}.

2.7. Motility, biofilm, self-aggregation

The swimming and swarming motility of both the WT and Δ*tspO* mutant strains were assessed on MODG plates containing 0.25% and 0.7% (w/v) Bacto-agar (Difco), respectively [25]. Cells were cultivated until reaching mid-log phase, and the OD_{600nm} was adjusted to 0.5. Subsequently, 2 μl of cell suspensions were applied to the center of MODG plates, followed by incubation at 37 °C. Motility was quantified based on the diameter of the growth halo.

Biofilm formation by *B. cereus* WT and Δ*tspO* mutant strains was determined using previously established methods [26]. Briefly, WT and Δ*tspO* cells were grown overnight at 37 °C in Brain Heart Infusion Broth medium. They were subsequently diluted to an OD_{600nm} of 1. A volume of 200 μl was dispensed into the wells of 96-well plates and left to incubate for 24 h at 37 °C without agitation. Biofilms were stained with 200 μL of 1% (w/v) crystal violet for 20 min, followed by a triple wash with PBS. The crystal violet, binding to the biofilm, was dissolved using 200 μL of 100% ethanol. Quantification of biofilms was performed by measuring the optical density resulting from the crystal violet at 590 nm.

For self-aggregation assays, cell suspensions of both WT and Δ*tspO* strains, collected from overnight cultures in MODG medium, were adjusted to an OD_{600nm} of approximately 1. A 1 mL aliquot of the culture suspension was then placed in a spectrophotometer cuvette, and the OD_{600} was monitored over a 4-h static incubation period. The results are expressed as a percentage of the initial OD_{600nm}.

2.8. Susceptibility to oxidizing agents

The impact of H_2O_2 (30%) and paraquat (5%) on the growth of both WT and Δ*tspO* strains was assessed through a disk diffusion assay. *B. cereus* strains were cultured overnight in MODG, and 100 μl of the culture was added to 4 mL of molten soft agar before being plated on MODG agar plates. Diffusion disks (6 mm, Whatman) loaded with 5 μl of oxidizing agents were placed on the plates, which were then incubated for 24 h at 37 °C. The zones of growth inhibition were subsequently recorded.

2.9. Oxygen consumption measurements

Oxygen consumption by cell suspension was measured at 37 °C in a 2-mL water-jacketed reaction chamber with a Clark-type electrode (Hansatech Instruments Ltd, Norfolk, UK). Aerobically grown bacteria in MODG culture media were diluted in the same culture media at an OD_{600nm} of 0.35–0.45 and 500 μl were incubated in a respiration stirred buffer (100 mM KCl, 50 mM sucrose, 10 mM HEPES and 5 mM KH_2PO_4, pH 7.4 at 30 °C). Oxygen consumption was measured for 2 min and then a complex inhibitor (50 μM rotenone, 1 mM malonate, 50 μM antimycin A or 4 mM KCN) or the uncoupling carbonyl cyanide p-(trifluoromethoxy)phenylhydrazone (10 μM FCCP) was added. Oxygen consumption was quantified by measuring the slopes of the curves.

2.10. Total porphyrin quantification, and specific porphyrin separation

Pellets of bacteria were homogenized in NaCl 0.9% and then sonicated. Total porphyrins were extracted from either bacterial lysates or the culture medium using ether–acetic acid (4/1, v/v). After centrifugation, HCl was added to the supernatant at a final concentration of 1 M. Following mixing, the lower acid layer was

collected. The total porphyrin fluorescence was detected by spectrofluorometry recording the excitation spectrum from 380 to 440 nm and measuring the emitted fluorescence at 602 nm. The concentration of porphyrins was estimated using a standard calibration.

Porphyrins isolated from the bacterial lysates and culture medium were converted into methyl esters through a reaction of an aqueous acid extract of porphyrins with methanol–sulfuric acid (95:5, v/v) in the dark at room temperature. Porphyrin methyl esters were extracted by adding chloroform and separated via normal-phase adsorption chromatography on a polar column (Silica, 10 μm, 30 cm × 3.9 mm; Waters μPorasil, Guyancourt, France) using a gradient of organic solvents (cyclohexane–ethyl acetate ranging from 62/38 to 40/60, v/v) for elution. The retention times increased as the number of ester side chains increased. Detection was performed using a fluorescence detector with an excitation wavelength at 400 nm and an emission wavelength at 630 nm.

2.11. Statistical analysis

All experiments were conducted with, at least, three biological replicates each. The data measured for the Δ*tspO* mutant and WT strains were compared using Student's *t*-test ($p \leq 0.05$ was considered significant). All analyses were performed using Prism5 (GraphPAd), and the data are represented as means ± S.E. of the mean.

3. Results

3.1. BcTSPO improves B. cereus respiratory growth

We constructed a Δ*tspO* null *B. cereus* strain by replacing the ORF encoding BcTSPO (BC_3136) by a spectinomycin-resistance cassette. On LB agar plates, Δ*tspO* colonies displayed a reduced size compared to WT colonies, suggesting impaired growth on solid medium (Fig. S1A). Moreover, the Δ*tspO* strain exhibited altered growth in both LB and MODG liquid media when cultivated in microplates (Figs. S1B and S1C). Interestingly, we observed that nutrient deprivation in MODG medium exacerbated the growth defect of the Δ*tspO* strain (Fig. S1). This growth impairment was rescued by introducing additional copies of the *tspO* genes in trans (Fig. S1). Subsequently, the Δ*tspO* mutant and WT strains were cultured in batch in MODG medium (Fig. S2), and their growth characteristics are detailed in Table 1. The results revealed that Δ*tspO* cells experienced a longer delay in growth, a lower growth rate, and increased final biomass compared to WT, with no significant change in the specific rate of glucose consumption. Moreover, it was noted that the final pH in Δ*tspO* mutant cells was less acidic than in the wild-type cells, potentially accounting for the elevated final biomass. While both Δ*tspO* and WT strains exhibited similar spectra of end by-products, the Δ*tspO* strain excreted less acetic acid than its parental strain, contributing to the observed increased in final pH. Given the absence of a shift toward fermentative metabolism and the reduced level of acetate overflow, these observations strongly suggest a disturbance or perturbation within the respiratory pathways when BcTSPO is lacking.

Table 1
Batch cultures results of the Δ*tspO* mutant and its parent strain *B. cereus* ATCC 14579.

Parameters and yield of end-products	WT	Δ*tspO*
Parameters		
λ (h^{-1})	0.36 ± 0.05	0.79 ± 0.22*
μ_{max} (h^{-1})	1.39 ± 0.04	1.05 ± 0.09*
Final OD_{600}	2.3 ± 0.0	3.2 ± 0.3*
Final pH	5.0 ± 0.0	6.2 ± 0.0*
Maximum glucose consumption rate (mM/OD/h)	5.13 ± 0.51	5.48 ± 0.42
Yields of end products (mol/mol of glucose)		
Acetate	0.93 ± 0.15	0.42 ± 0.07*
Lactate	0.20 ± 0.02	0.18 ± 0.02
Succinate	0.03 ± 0.00	0.03 ± 0.00
Ethanol	NZ	NZ
Formate	NZ	NZ

*significantly different compared to WT ($p < 0.05$).
NZ: near zero.

3.2. Phosphate starvation responsive proteins participate to cellular proteome remodeling in Δ*tspO* cells

To investigate the cellular response to BcTSPO deprivation, we compared the cellular proteome of Δ*tspO* and WT cells collected during the exponential growth phase ($OD_{600} = 0.2$; Fig. S2). In total, 25405 peptide sequences were observed certifying the presence of 1794 cellular proteins, which were identified by at least two distinct peptides across all 6 samples analyzed (2 strains x 3 biological replicates, Table S2). Principal component analysis revealed good homogeneity of the biological triplicates for the two strains, and showed that the cellular proteome of *B. cereus* was remodeled in the absence of BcTSPO (Fig. S3). Differential analysis identified 256 proteins with significantly different abundances (|fold-change| ≥ 1.5, *p*-value ≤0.05, Table S3) in Δ*tspO* compared to WT. Among these differentially accumulated proteins (DAPs), 108 were detected at lower levels in Δ*tspO* compared to WT (down-DAPs), whereas 158 were detected at higher levels (up-DAPs) (Table S3, Fig. 1A). Functional classification of DAPs by COG (Cluster of Orthologous Groups of proteins) indicated that up-DAPs were primarily associated with amino acid and energy metabolism, while down-regulated DAPs were linked to cellular processes, signaling, and, to a lesser extent, information storage and processing (including translation and replication factors) (Fig. 1B). This suggests that Δ*tspO* cells require increased translational capacity for primary/energy metabolism, potentially affecting biomass formation, envelope biogenesis, motility, and virulence. DAPs were further analyzed by gene ontology (GO) pathway enrichment analysis. The results showed that the tryptophan biosynthetic pathway and the tricarboxylic acid cycle (TCA) cycle are the metabolic pathways mainly up-regulated in *ΔtspO* cells (Fig. 1C).

Several transcriptional regulators exhibited increased abundance levels in *ΔtspO* cells when compared to the WT (Table S3). Notably, among these regulators is the two-component system PhoP-PhoR (BC_4588-BC_4589), responsible for governing the Pho Regulon, which becomes activated in response to inorganic phosphate scarcity. The Pho regulon oversees a spectrum of cellular functions, including carbon and energy metabolism, secondary metabolite production, cell wall integrity, motility, and pathogenesis [27,28]. Interestingly, we observed that PhoH (BC_4502), PhoU (BC_4265), PstB (BC_4266) integral components of the Pi starvation response, also exhibited significantly increased abundance levels in *ΔtspO* cells in comparison to the WT (Table S3).

Furthermore, additional regulators with elevated abundance levels in *ΔtspO* cells include the two-component response regulator WalK-WalR (BC_4810), which plays a crucial role in cell wall metabolism [29], the σ54-dependent transcriptional activator (BC_4165), controlling various physiological processes such as the utilization of alternative carbon sources and the regulation of detoxification systems, along with the assembly of motility-related structures [30]. Additionally, the Hut operon positive regulatory protein (HutP, BC_3653), responsible for overseeing the degradation of histidine, was found to be among the regulators exhibiting increased abundance levels [31]. These findings collectively indicate that *B. cereus* responds to the absence of BcTSPO by

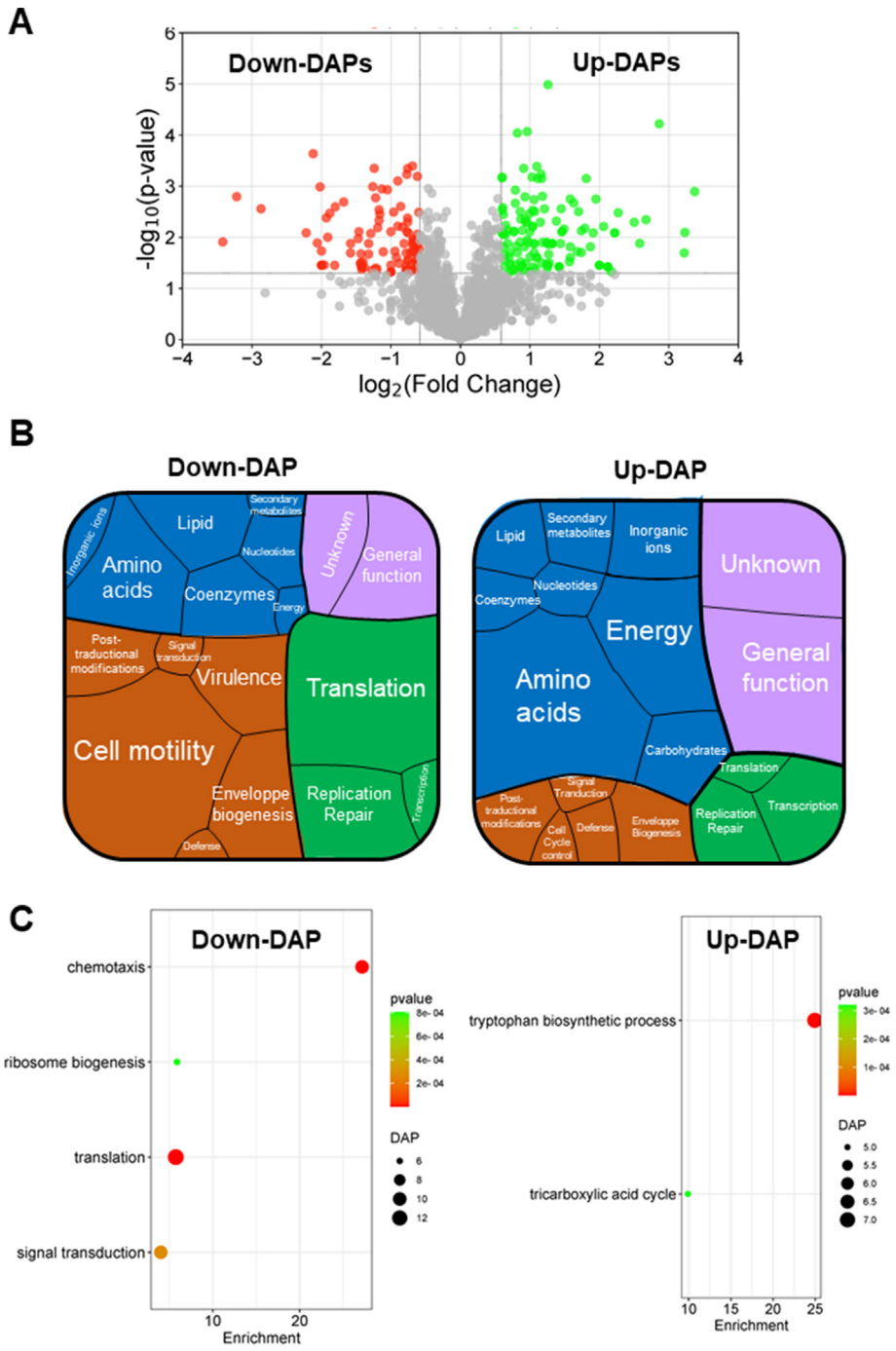

Fig. 1. Comparative Analysis of Differentially Accumulated Proteins (DAPs) between WT and Δ*tspO* strains. **A.** Volcano plot for the comparison between WT and Δ*tspO* strains. The cutoff values fold change >1.5 and *p*-value <0.05 were utilized to identify DAPs. Proteins with no significant changes in abundance levels are depicted in gray. Red color is indicative of down-DAPs and green is indicative of up-DAPs. **B**. Voronoï tree map showing clusters of orthologous protein groups (COGs) in which down-DAPs and up-DAPs are involved. COG groups associated with metabolism are highlighted in blue, those linked to cellular processes and signaling in orange, those involved in information storage and processing in green, and those pertaining to poorly characterized processes in purple. **C**. Gene ontology (GO) enrichment of up- and down DAPs.

reprogramming its cellular functions.

3.3. *BcTSPO improves B. cereus cell motility, auto-aggregation and biofilm formation*

Whole cell proteome showed lower accumulation of twenty flagellar and chemotaxis-related proteins in the *ΔtspO* strain compared to WT. These proteins encompass a wide range of flagellar components, including cytoplasmic chaperones, structural proteins of the basal body, and flagella filament proteins. Additionally, they involve methyl-accepting chemotaxis proteins and proteins responsible for the transduction of chemotactic signals (Table S3). These results prompted us to evaluate whether *ΔtspO* cells displayed altered motility behavior. Δ*tspO* cells exhibit significantly reduced swarming motility (Fig. 2A) compared to WT cells on MODG agar medium, but not swimming motility (Fig. 2B)

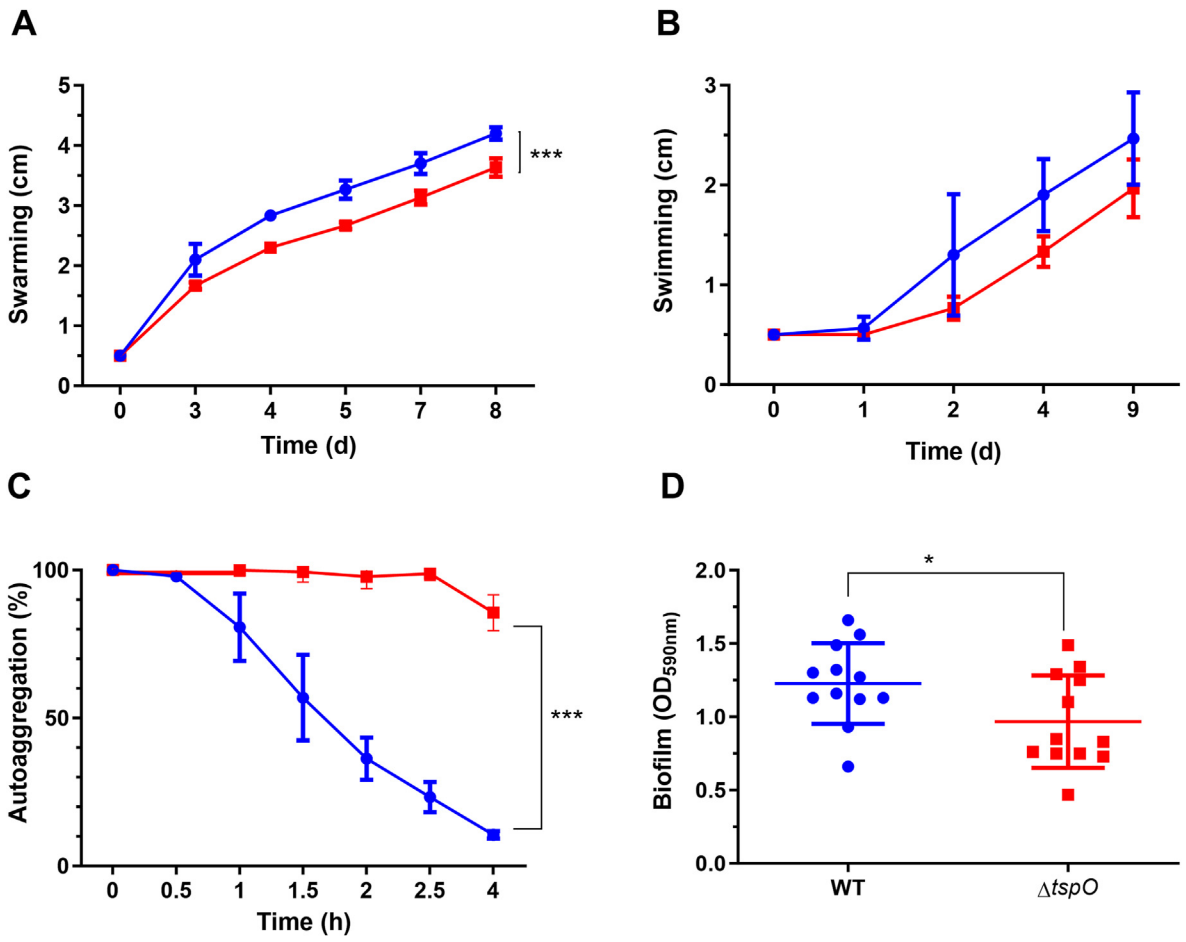

Fig. 2. Characterization of phenotypic traits in WT (blue) and Δ*tspO* (red) strains. **A**. Swarming motility of WT and Δ*tspO* strains. Diameters of motility halos were measured on MODG plates containing 0.7% agar. **B**. Swimming motility of WT and Δ*tspO* strains. Diameters of motility halos were measured on MODG plates containing 0.3% agar. **C**. Autoaggregation capacity of WT and Δ*tspO* strains. **D**. Biofilm formation measured by crystal violet absorbance at 590 nm in WT and Δ*tspO* strains. A two-way repeated measures ANOVA was utilized to assess significant differences in motility and autoaggregation between the WT and Δ*tspO* strains. A Student's t-test was employed to determine significant differences in biofilm formation. *, $p < 0.05$, ***, $p < 0.001$.

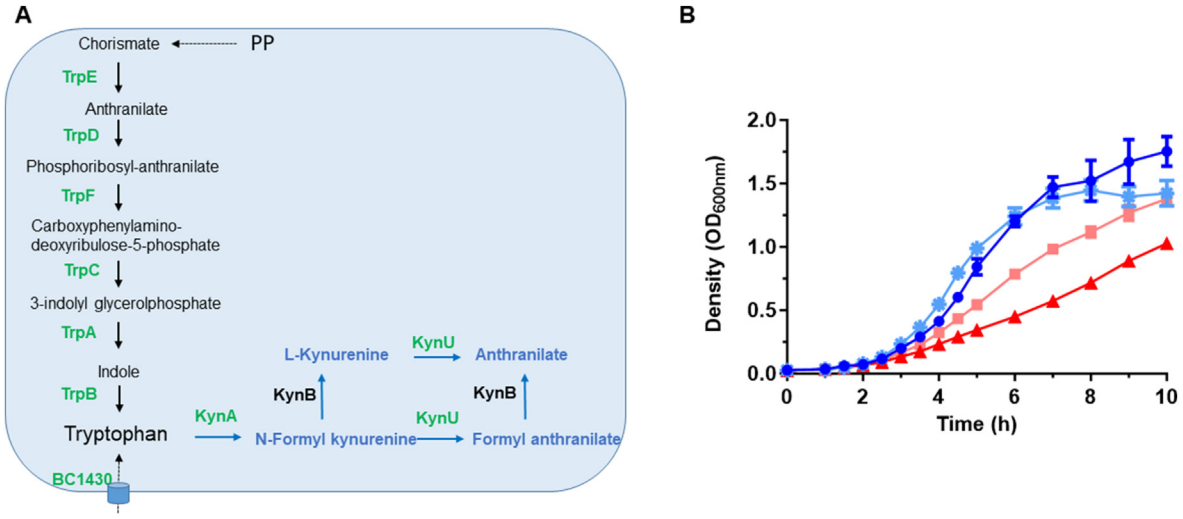

Fig. 3. Impact of Δ*tspO* mutation on tryptophan pathways and growth dynamics in MODG medium. **A**. Tryptophan biosynthesis and degradation pathways. Proteins up-regulated in Δ*tspO* compared to WT are indicated in green. Proteins not modified are indicated in black. PP, pentose phosphate pathway; TrpE, anthranilate synthase; TrpD, anthranilate phosphoribosyltransferase; TrpF, phosphoribosyl antranilate isomerase; TrpC, indol-3-glycerol phosphate synthase; TrpB, TrpA, tryptophane synthases; KynA, tryptophan 2,3-dioxygenase; KynU, kynureninase; KynB, kynurenine formamidase. BC_1430, sodium-dependent tryptophan transporter. **B.** Growth curves of Δ*tspO* and WT strains in MODG medium supplemented (square and star symbols) or not (triangle and circle symbols) with tryptophan (1 g/L). Square symbols represent Δ*tspO* strain supplemented with tryptophan, while triangle symbols represent Δ*tspO* strain without tryptophan. Star symbols denote WT strain with tryptophan supplementation, and circle symbols represent WT strain without tryptophan. WT strain is indicated in blue, and Δ*tspO* strain in red.

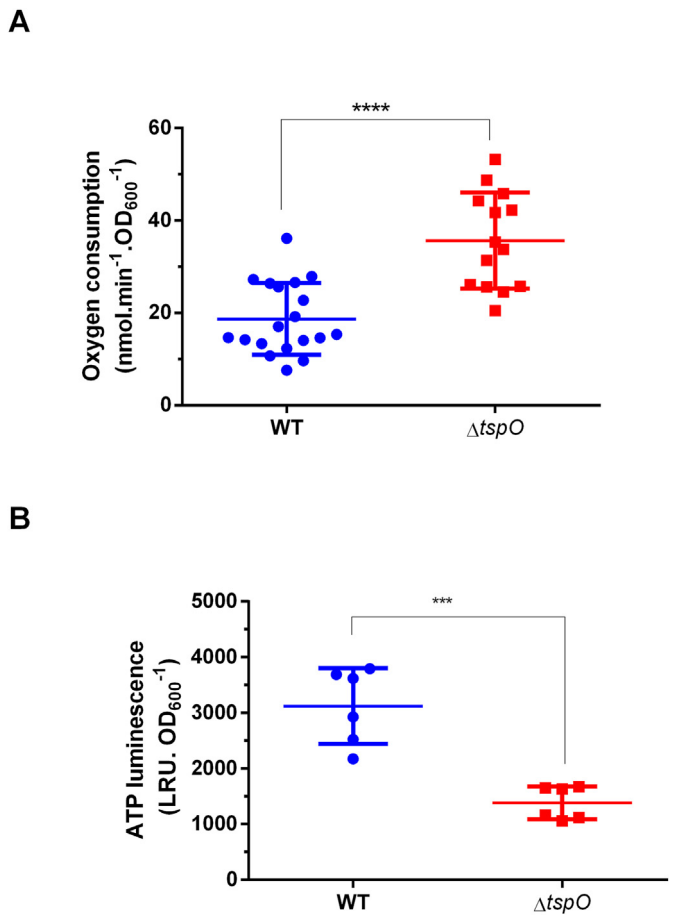

Fig. 4. Oxygen consumption rate and ATP production levels of WT and Δ*tspO* cells grown on MODG medium. **A**. Oxygen consumption. Values represent the mean of 19 measurements for WT cells and 14 measurements for Δ*tspO* cells. **B**. ATP production. The luminescence intensity, expressed as Luminescence Relative Units (LRU), correlates with ATP quantity. Statistical analysis was conducted using a Student's t-test. ***, $p < 0.001$; ****, $p < 0.0001$.

on MODG agar medium. In *B. cereus*, motility, auto-aggregation, and biofilm formation are interconnected biological processes. Therefore, we investigated the impact of the Δ*tspO* null mutation on *B. cereus*' ability to auto-aggregate and form biofilms. Sedimentation kinetics revealed that Δ*tspO* cells displayed poor aggregation, with only 14.4% ± 6.0% auto-aggregation after 4 h, while WT cells rapidly auto-aggregated (Fig. 2C). Quantitative analysis of biofilm formation through a crystal violet assay indicated that Δ*tspO* cells formed fewer biofilms than WT cells (Fig. 2D). In conclusion, it appears that BcTSPO regulates motility, auto-aggregation and biofilm formation in *B. cereus*.

3.4. BcTSPO regulates kynurenine/anthranilate pathway of tryptophan metabolism

Proteome analysis revealed the following findings in the Δ*tspO* mutant compared to the WT strain: (i) A higher accumulation of the seven enzymes responsible for the synthesis of tryptophan from chorismate; (ii) Increased levels of a sodium-dependent tryptophan transporter; (iii) higher accumulation of enzymes such as tryptophan 2,3-dioxygenase (Kyn A) and kynureninase (Kyn U), which are involved in the initial and third steps of tryptophan catabolism into anthranilate (Fig. 3A). These results suggest that Δ*tspO* cells support enhanced degradation of tryptophan, consequently necessitating increased tryptophan synthesis. To ascertain whether a depletion of tryptophan contributes to the growth defect in Δ*tspO* cells, we supplemented the MODG growth medium with tryptophan (1 g/L) and compared the growth of Δ*tspO* and WT strains (Fig. 3B). The results indicated that the addition of tryptophan partially rescued the growth deficiency of the Δ*tspO* mutant.

3.5. BcTSPO regulates energy metabolism and ROS production in B. cereus

The increased accumulation in Δ*tspO* cells of citrate synthase (CitZ), malate quinone oxidoreductase (Mqo) that is part of both TCA and electron transport chain, succinyl CoA ligase subunits α and β (SucC and SucD), and malate dehydrogenase (Mdh) (Table S3) suggests an upregulation of TCA activity in Δ*tspO* cells. To determine whether the dysfunction of the TCA cycle in Δ*tspO* cells is accompanied by alterations in the oxidative phosphorylation respiratory chain, we measured the basal oxygen consumption in Δ*tspO* and WT strains. The results showed that Δ*tspO* cells consume higher levels of oxygen compared to WT cells (Fig. 4A). Additionally, measurements of ATP production revealed that the Δ*tspO* mutant has significantly reduced ATP production (Fig. 4B). Taken together, these results suggest that the lack of BcTSPO alters the coupling between electron transport and ATP synthesis. Dysfunction of oxidative phosphorylation generates high levels of ROS, leading to the prediction that Δ*tspO* cells may produce high levels of ROS. Consistent with this prediction, our proteomic analysis revealed increased levels of proteins associated with the oxidative stress response in Δ*tspO* compared to WT cells (Table S3). We found that Δ*tspO* cells indeed produce increased levels of ROS (Fig. 5A), and increased catalase activity (Fig. 5B). To further test whether elevated endogenous ROS levels may limit the antioxidant system's defense, we compared the resistance of Δ*tspO* and WT cells to oxidative stress induced by H_2O_2 and paraquat (Fig. 5C and D). The results indicate that Δ*tspO* cells are less resistant to oxidative stress than WT cells.

3.6. BcTSPO regulates free porphyrin levels

Our proteomic analysis unveiled an increased presence of coproporphyrin ferrochelatase (CpfC2) within the Δ*tspO* mutant cells compared to the WT (Table S3), indicating an escalated porphyrin flux at this pivotal juncture of the heme biosynthetic pathway (Fig. 6A). We conducted quantification of intracellular and secreted porphyrin levels in both Δ*tspO* and WT cells. Fig. 6B illustrates that, overall, porphyrins accumulate to a greater extent within the Δ*tspO* cells, accompanied by elevated levels found outside the cells. However, the ratio of internal to external accumulation (3 ± 1 for Δ*tspO* cells vs. 7 ± 4 for WT) was not significantly different. Remarkably, neither WT nor Δ*tspO* mutant cells showed detectable levels of protoporphyrin (Fig. 6C), which aligns with the predominant utilization of the coproporphyrin-dependent branch (CPD) in the heme biosynthetic pathway by *B. cereus* [32]. Coproporphyrin predominates in WT strain. In contrast, within the Δ*tspO* mutant strain, uroporphyrin, 5-carboxyporphyrin (5-COOH), and 7-carboxyporphyrin (7-COOH) exhibit similar levels of accumulation as coproporphyrin, whereas the presence of 6-carboxyporphyrin (6-COOH) is nearly half that of coproporphyrin (Fig. 6C). This diverse pattern underscores a significant increase in heme *b* precursors within the Δ*tspO* mutant strain compared to the WT, particularly within the cells. These observations strongly suggest the involvement of BcTSPO in the synthesis pathway of heme *b*.

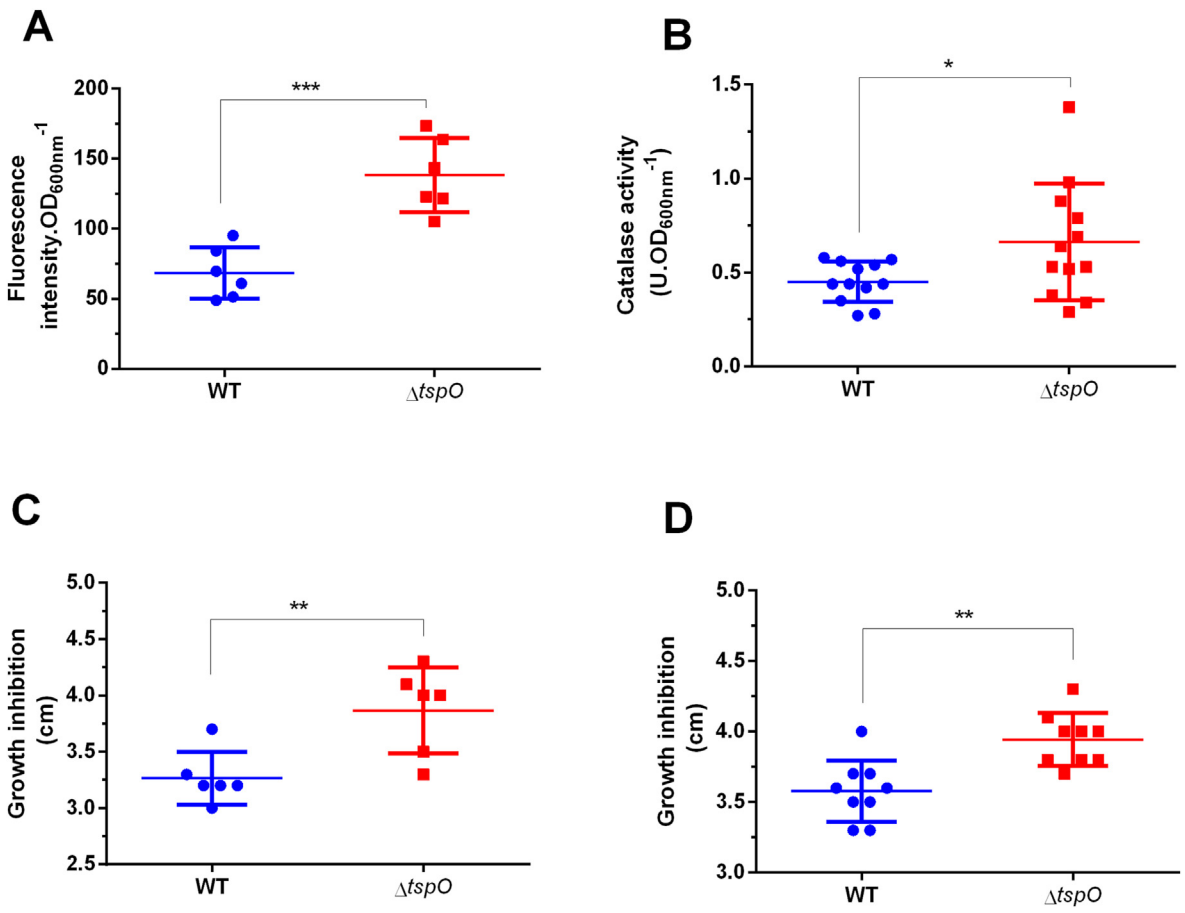

Fig. 5. Comparative analysis of oxidative stress response in WT and Δ*tspO* cells grown on MODG medium. **A**. Quantification of ROS production using fluorescent dye DCFDA as an indicator of oxidative stress. **B**. *Measurement of catalase activity* via *decrease in* H_2O_2 absorbance at 240 nm. **C**. Assessment of resistance and susceptibility to H_2O_2 (30%). **D**. Evaluation of resistance and susceptibility to methylviologen (Paraquat, 5%). Statistical analysis was conducted using a Student's t-test *, $p < 0.05$; **, $p < 0.01$; ***, $p < 0.001$; ****, $p < 0.0001$.

4. Discussion

In a previous study, the degradation of porphyrins by recombinant BcTSPO was demonstrated, suggesting its physiological significance in protecting against oxidative stress [17]. Our current work reveals BcTSPO as a pivotal component in aerobic respiratory metabolism, motility, and biofilm formation, and a potential factor contributing to the virulence of *B. cereus*.

Our finding reveal that the absence of BcTSPO leads to a depletion of cellular ATP despite an increase in oxygen flow through the respiratory chain. This suggests a potential alteration in ATP synthase-ATPase activity [35]. The efficiency of ATP synthesis by the ATP-synthase complex may be diminished in the absence of TSPO due to a redirection of electron transport towards the less energy-efficient cytochrome *bd* oxidase termination branch, at the expense of the energy-efficient cytochrome *aa3*-termination branch of the respiratory chain cytochromes [36–38]. However, this hypothesis lacked support from proteomics data, as the CydA and CydB integral membrane components of cytochrome *bd* oxidase were undetectable due to their hydrophobic properties. ATP-synthase decoupling could also stem from increased demand for ATP in tryptophan synthesis [39], or from membrane disorganization due to the absence of BcTSPO [40]. Additionally, the absence of BcTSPO notably increases ROS formation, possibly due to impairment of oxidative phosphorylation [33,34]. This heightened ROS production seems to overwhelm the antioxidant system, including proteins related to oxidative stress response like Q81E75 and Q81EL7 (Table S3), thus diminishing its effectiveness in combating exogenous stress [41,42].

The Δ*tspO* mutant cells respond to ATP depletion by activating the phosphate starvation response through the PhoP-PhoR two-component system. This adaptive response is recognized for reducing ATP-consuming processes like ribosomal synthesis, translation, motility, and enterotoxin synthesis [27,43]. The decrease in enterotoxin production in the Δ*tspO* mutant was supported by the reduced expression of the HBL-lytic and binding component L2, L1, B and B' (BC_3101, BC_3102, BC_3103, BC_3104) and NHE-lytic component L2 (BC1809, Table S3). Notably, the down-regulation of PapR, the quorum sensing effector of the pleiotropic regulator of virulence PlcR [44], was also observed in the Δ*tspO* mutant. The significant alteration in expression of the σ_{54} regulator in Δ*tspO* mutant cells could also contributed to the adaptive response to ATP depletion [45]. This regulator governs carbohydrate metabolism, motility, biofilm formation, and PlcR/PapR-dependent enterotoxin production [46]. In cells with limited phosphate, PhoP-PhoR and WalK-WalR jointly regulate cell wall metabolism and biofilm formation [47]. We observed an up-regulation of both these components in the Δ*tspO* mutant cells, possibly indicating their collaborative role. Hence, the adaptive response to Δ*tspO* -induced ATP depletion is intricate and likely involves several broad-reaching regulators and two-component systems.

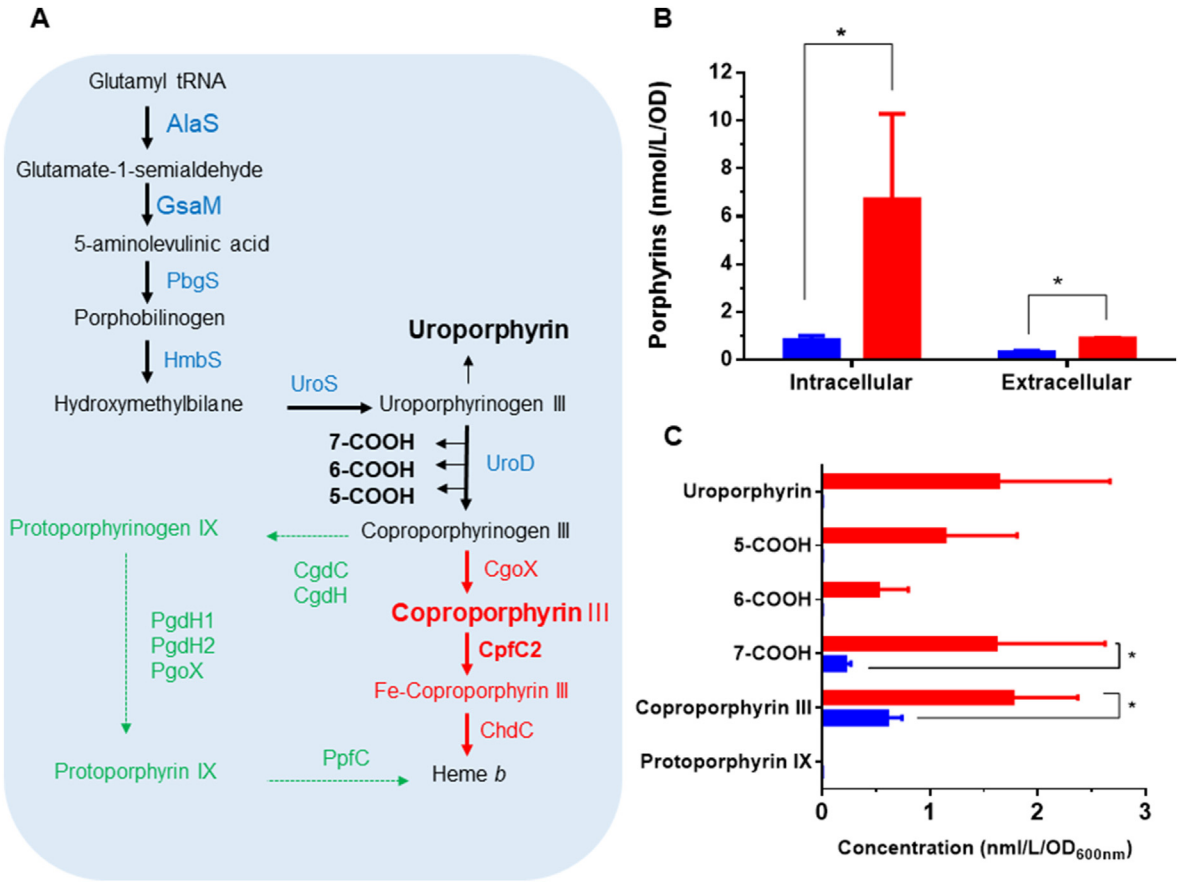

Fig. 6. Comparative analysis of porphyrin biosynthesis and distribution in *B. cereus* WT and Δ*tspO* cells. **A**. *B. cereus* metabolic pathway leading to heme *b* synthesis. AlaS, glutamyl-tRNA-reductase, GsaM, glutamate-1-semialdhehyde 2,1 aminomutase; PbgS, porphobilinogen synthase; HmbS, porphobilinogen deaminase; UroS, Uroporphyrin-III C-methyl-transferase; UroD, Uroporphyrinogen decarboxylase; CgoX, coproporphyrinogen III oxidase; CpfC2, coproporphyrin ferrochelatase 2; ChdC, coproheme decarboxylase; CgdC, coproporphyrinogen decarboxylase; CgdH, coproporphyrinogen dehydrogenase; PgdH1 and PgdH2, protoporphyrinogen dehydrogenase; PgoX, protoporphyrinogen oxidase; PpfC, protoporphyrin ferrochelatase. Coproporphyrin dependent pathway is indicated in red, and protoporphyrin dependent pathway is indicated in green. CpfC2, which showed increased level in Δ*tspO* mutant cells compared to WT is in bold. **B**. Intracellular production and extracellular excretion of total porphyrins in WT (blue) and Δ*tspO* (red) cells. **C**. Intracellular porphyrin composition. 5-COOH, 5-carboxyporphyrin, 6-COOH, 6-carboxyporphyrin and 7-COOH, 7-carboxyporphyrin. Statistical analysis was conducted using a Student's t-test *, $p < 0.05$.

Our research findings reveal that BcTSPO also acts as a modulator of tryptophan metabolism. It limits its oxidative degradation through the kynurenine/anthranilate pathway (Fig. 3) [48]. This inhibition of the degradation process boosts protein synthesis, thereby prioritizing cellular growth. Tryptophan has also been observed to disrupt the quorum-sensing abilities of *B. subtilis*, consequently regulating its biofilm formation [49]. Consistent with the interference in quorum sensing, the abundance of the quorum-sensing effector PapR was found to notably increase in Δ*tspO* cells. *B. cereus* degrades tryptophan into anthranilate [50], a compound known to impede biofilm formation in various bacteria [51]. Therefore, the action of BcTSPO indirectly supports both growth and biofilm formation through the regulation of tryptophan metabolism.

Our findings strongly suggest that BcTSPO plays a crucial role in controlling free porphyrin levels. This is supported by the notable increase in the accumulation of metabolites of the CPD branch of heme biosynthesis pathway in the Δ*tspO* cells compared to the WT cells. Correspondingly, the heightened synthesis of CpfC2 in the Δ*tspO* cells aligns with its role in promoting the insertion of ferrous ions into coproporphyrin, a process associated with modulating porphyrin accumulation in *B. subtilis* [52]. Studies in *S. aureus* suggested that CpfC interacts with coproheme decarboxylase CdhC, that decarboxylates coproheme to generate heme *b* [53]. Increased level of CpfC may thus facilitate heme *b* production via CdhC for proteins that rely on it as a prosthetic group. Among these proteins are CpfC2 itself, respiratory cytochromes, cytochrome P450 (such as BC_2609, Table S3), catalase, and tryptophan 2, 3-dioxygenase (KynA, Fig. 3A). Our findings reveal either an overproduction of these enzymes or alterations in pathways in which these enzymes are involved. This strongly suggests that in response to BcTSPO-induced porphyrin accumulation, *B. cereus* activates pathways connected to heme utilization. This activation might serve as a compensatory mechanism aimed at managing the heightened porphyrin levels. In summary, our findings propose that BcTSPO indirectly influences energy metabolism, oxidative stress response, tryptophan metabolism, and subsequently, crucial aspects such as growth, motility, biofilm formation, and virulence in *B. cereus*. This influence stems from its role in maintaining low levels of free porphyrins.

The precise mechanism through which BcTSPO regulates the levels of metabolites in the CPD branch of heme biosynthesis pathway remains a topic of ongoing investigation. One hypothesis suggests that BcTSPO could potentially interact with the final three enzymes—CgoX, CpfC, and ChbC—involved in the heme biosynthesis pathway (Fig. 6A). In Gram-positive bacteria, these enzymes are not bound to membranes [54], and it has been proposed that their transient interaction might offer an alternative to membrane

compartmentalization for regulating porphyrin flux [53,55]. By forming a complex with CgoX, CpfC, and ChbC, BcTSPO could potentially facilitate substrate channeling within the heme biosynthetic pathway or affect the release of intermediates from this pathway. Notably, the documented interactions of TSPO with CogX in *R. sphaeroides*, *Sinorhizobium meliloti*, *Pseudomonas* [56,57], along with its demonstrated capability to scavenge and degrade porphyrins [18,58], support this hypothesis.

5. Conclusion

TSPO has primarily been studied in mammals, with more limited exploration in plants, invertebrates, and bacteria. In *Arabidopsis thaliana* TSPO is stress-induced [59], binds porphyrins and regulates heme content [60]. Among bacteria, the investigation of TSPO has predominantly focused on Gram-negative species. We showed that in the gram-positive pathogen *B. cereus*, BcTSPO assumes a crucial role in energy metabolism, akin to its mammalian counterparts [2]. Moreover, it regulates the tryptophan kynurenine pathway, a function not previously described in mammals. The kynurenine pathway in *B. cereus* shares commonalities with that of mammals. Specifically, tryptophan-2, 3-dioxygenase (KynA, TDO), potentially regulated by BcTSPO in *B. cereus*, governs the initial and rate-limiting step in both the *B. cereus* and mammalian kynurenine pathways. In mammals, TDO, along with metabolites from the kynurenine pathway, has been directly or indirectly associated with various conditions, including inflammatory diseases, cancer, diabetes, and mental disorders [61,62]. This newfound function of TSPO identified in *B. cereus* thus opens novel perspectives regarding its role in mammals. Furthermore, studies confirming an interaction between BcTSPO and enzymes involved in the heme biosynthesis pathway could shed light on potential functions of TSPO in eukaryotes.

Author contributions

Catherine Duport: Conceptualization, Methodology, Validation, Formal analysis, Investigation, Data curation, Writing - original draft, Writing - review & editing, Supervision. Jean Armengaud: Methodology, Validation, Writing - review & editing. Caroline Schmitt: Methodology, Validation, Writing - review & editing. Didier Morin: Methodology, Validation, Writing - review & editing, Jean-Jacques Lacapère: Methodology, Validation, Writing - review & editing, Supervision.

Declaration of competing interest

The authors declare no competing interests.

Acknowledgements

We thank Justine Thorel for her technical help, and Mélodie Kielbasa (ProGénoMix platform) for performing the tandem mass spectrometry measurements. This work was funded by Avignon University.

Appendix A. Supplementary data

Supplementary data to this article can be found online at https://doi.org/10.1016/j.biochi.2024.02.008.

References

[1] V. Papadopoulos, M. Baraldi, T.R. Guilarte, T.B. Knudsen, et al., Translocator protein (18kDa): new nomenclature for the peripheral-type benzodiazepine receptor based on its structure and molecular function, Trends Pharmacol. Sci. 27 (2006) 402–409.
[2] C. Hiser, B.L. Montgomery, S. Ferguson-Miller, TSPO protein binding partners in bacteria, animals, and plants, J. Bioenerg. Biomembr. 53 (2021) 463–487.
[3] J.-J. Lacapere, L. Duma, S. Finet, M. Kassiou, V. Papadopoulos, Insight into the structural features of TSPO: implications for drug development, Trends Pharmacol. Sci. 41 (2020) 110–122.
[4] H. Batoko, V. Veljanovski, P. Jurkiewicz, Enigmatic Translocator protein (TSPO) and cellular stress regulation, Trends Biochem. Sci. 40 (2015) 497–503.
[5] J. Fan, M.B. Rone, V. Papadopoulos, Translocator protein 2 is involved in cholesterol redistribution during erythropoiesis, J. Biol. Chem. 284 (2009) 30484–30497.
[6] F. Li, J. Liu, N. Liu, L.A. Kuhn, et al., Translocator protein 18 kDa (TSPO): an old protein with new functions? Biochemistry 55 (2016) 2821–2831.
[7] A.A. Yeliseev, S. Kaplan, A sensory transducer homologous to the mammalian peripheral-type benzodiazepine receptor regulates photosynthetic membrane complex formation in *Rhodobacter sphaeroides* 2.4.1, J. Biol. Chem. 270 (1995) 21167–21175.
[8] X. Zeng, S. Kaplan, TspO as a modulator of the repressor/antirepressor (PpsR/AppA) regulatory system in *Rhodobacter sphaeroides* 2.4.1, J. Bacteriol. 183 (2001) 6355–6364.
[9] M.E. Davey, F.J. de Bruijn, A homologue of the tryptophan-rich sensory protein TspO and FixL regulate a novel nutrient deprivation-induced *Sinorhizobium meliloti* locus, Appl. Environ. Microbiol. 66 (2000) 5353–5359.
[10] C. Leneveu-Jenvrin, E. Bouffartigues, O. Maillot, P. Cornelis, et al., Expression of the translocator protein (TSPO) from *Pseudomonas fluorescens* Pf0-1 requires the stress regulatory sigma factors AlgU and RpoH, Front. Microbiol. 6 (2015).
[11] A.W.U. Busch, Z. WareJoncas, B.L. Montgomery, Tryptophan-rich sensory protein/translocator protein (TSPO) from cyanobacterium *Fremyella diplosiphon* binds a broad range of functionally relevant tetrapyrroles, Biochemistry 56 (2017) 73–84.
[12] M. Ehling-Schulz, D. Lereclus, T.M. Koehler, The *Bacillus cereus* group: Bacillus species with pathogenic potential, Microbiol. Spectr. 7 (2019).
[13] Y. Liu, J. Du, Q. Lai, R. Zeng, et al., Proposal of nine novel species of the *Bacillus cereus* group, Int. J. Syst. Evol. Microbiol. 67 (2017) 2499–2508.
[14] J. Jovanovic, V.F.M. Ornelis, A. Madder, A. Rajkovic, *Bacillus cereus* food intoxication and toxicoinfection, Compr. Rev. Food Sci. Food Saf. 20 (2021) 3719–3761.
[15] C. Duport, M. Jobin, P. Schmitt, Adaptation in *Bacillus cereus*: from stress to disease, Front. Microbiol. 7 (2016) 1550.
[16] N. Ivanova, A. Sorokin, I. Anderson, N. Galleron, et al., Genome sequence of *Bacillus cereus* and comparative analysis with *Bacillus anthracis*, Nature 423 (2003) 87–91.
[17] Y. Guo, R.C. Kalathur, Q. Liu, B. Kloss, et al., Structure and activity of tryptophan-rich TSPO translocator proteins, Science 347 (2015) 551–555.
[18] L. Issop, L. Duma, S. Finet, O. Lequin, J.-J. Lacapere, Among the recombinant TSPOs, the BcTSPO, Biochimie S0300-9084 (24) (2024), https://doi.org/10.1016/j.biochi.2024.01.011, 00029-4.
[19] E. Rosenfeld, C. Duport, A. Zigha, P. Schmitt, Characterization of aerobic and anaerobic vegetative growth of the food-borne pathogen *Bacillus cereus* F4430/73 strain, Can. J. Microbiol. 51 (2005) 149–158.
[20] M.H. Zwietering, I. Jongenburger, F.M. Rombouts, K. van 't Riet, Modeling of the bacterial growth curve, Appl. Environ. Microbiol. 56 (1990) 1875–1881.
[21] J.-P. Madeira, B. Alpha-Bazin, J. Armengaud, C. Duport, Time dynamics of the *Bacillus cereus* exoproteome are shaped by cellular oxidation, Front. Microbiol. 6 (2015) 342.
[22] V. Dupierris, C. Masselon, M. Court, S. Kieffer-Jaquinod, C. Bruley, A toolbox for validation of mass spectrometry peptides identification and generation of database: IRMa, Bioinformatics 25 (2009) 1980–1981.
[23] P.C. Carvalho, J.R. Yates III, V.C. Barbosa, Improving the TFold test for differential shotgun proteomics, Bioinformatics 28 (2012) 1652–1654.
[24] Y. Hanaoka, I. Yumoto, Manipulation of culture conditions for extensive extracellular catalase production by *Exiguobacterium oxidotolerans* T-2-2T, Ann. Microbiol. 65 (2015) 1183–1187.
[25] S. Salvetti, E. Ghelardi, F. Celandroni, M. Ceragioli, et al., FlhF, a signal recognition particle-like GTPase, is involved in the regulation of flagellar arrangement, motility behaviour and protein secretion in *Bacillus cereus*, Microbiology (Read.) 153 (2007) 2541–2552.
[26] H. Omer, B. Alpha-Bazin, J.-L. Brunet, J. Armengaud, C. Duport, Proteomics identifies *Bacillus cereus* EntD as a pivotal protein for the production of numerous virulence factors, Front. Microbiol. 6 (2015) 1004.
[27] H. Antelmann, C. Scharf, M. Hecker, Phosphate starvation-inducible proteins of *Bacillus subtilis*: proteomics and transcriptional analysis, J. Bacteriol. 182 (2000) 4478–4490.
[28] F. Santos-Beneit, The Pho regulon: a huge regulatory network in bacteria, Front. Microbiol. 6 (2015).
[29] H. Takada, H. Yoshikawa, Essentiality and function of WalK/WalR two-component system: the past, present, and future of research, Biosci., Biotechnol., Biochem. 82 (2018) 741–751.
[30] V. Shingler, Signal sensory systems that impact σ54-dependent transcription, FEMS (Fed. Eur. Microbiol. Soc.) Microbiol. Rev. 35 (2011) 425–440.
[31] R.A. Bender, Regulation of the histidine utilization (Hut) system in bacteria, Microbiol. Mol. Biol. Rev. 76 (2012) 565–584.
[32] Y. Nitzan, M. Salmon-Divon, E. Shporen, Z. Malik, ALA induced photodynamic effects on Gram positive and negative bacteria, Photochem. Photobiol. Sci. 3

(2004) 430–435.
[33] P. Millard, B. Enjalbert, S. Uttenweiler-Joseph, J.-C. Portais, F. Létisse, Control and regulation of acetate overflow in *Escherichia coli*, Elife 10 (2021) e63661.
[34] R.-Z. Zhao, S. Jiang, L. Zhang, Z.-B. Yu, Mitochondrial electron transport chain, ROS generation and uncoupling, Int. J. Mol. Med. 44 (2019) 3–15.
[35] T.V. Zharova, A.D. Vinogradov, Energy-dependent transformation of F0·F1-ATPase in *Paracoccus denitrificans* plasma membranes, J. Biol. Chem. 279 (2004) 12319–12324.
[36] A. Chateau, B. Alpha-Bazin, J. Armengaud, C. Duport, Heme A synthase deficiency affects the ability of *Bacillus cereus* to adapt to a nutrient-limited environment, Int. J. Mol. Sci. 23 (2022) 1033.
[37] T. Friedrich, D. Wohlwend, V.B. Borisov, Recent advances in structural studies of cytochrome *bd* and its potential application as a drug target, Int. J. Mol. Sci. 23 (2022) 3166.
[38] U. Kalnenieks, E. Balodite, R. Rutkis, Metabolic engineering of bacterial respiration: high vs. Low P/O and the case of *Zymomonas mobilis*, Front. Bioeng. Biotechnol. 7 (2019).
[39] T. Schuhmacher, M. Löffler, T. Hurler, R. Takors, Phosphate limited fed-batch processes: impact on carbon usage and energy metabolism in *Escherichia coli*, J. Biotechnol. 190 (2014) 96–104.
[40] V. Shoshan-Barmatz, S. Pittala, D. Mizrachi, VDAC1 and the TSPO: expression, interactions, and associated functions in health and disease states, Int. J. Mol. Sci. 20 (2019) 3348.
[41] M. Sharifi-Rad, N.V. Anil Kumar, P. Zucca, E.M. Varoni, et al., Lifestyle, oxidative stress, and antioxidants: back and forth in the pathophysiology of chronic diseases, Front. Physiol. 11 (2020) 694.
[42] A. Baez, J. Shiloach, Effect of elevated oxygen concentration on bacteria, yeasts, and cells propagated for production of biological compounds, Microb. Cell Factories 13 (2014) 181.
[43] N.E.E. Allenby, N. O'Connor, Z. Prágai, A.C. Ward, et al., Genome-wide transcriptional analysis of the phosphate starvation stimulon of *Bacillus subtilis*, J. Bacteriol. 187 (2005) 8063–8080.
[44] L. Slamti, D. Lereclus, Specificity and polymorphism of the PlcR-PapR quorum-sensing system in the *Bacillus cereus* group, J. Bacteriol. 187 (2005) 1182.
[45] M. Bush, R. Dixon, The role of bacterial enhancer binding proteins as specialized activators of σ54-dependent transcription, Microbiol. Mol. Biol. Rev. 76 (2012) 497–529.
[46] H. Hayrapetyan, M. Tempelaars, M. Nierop Groot, T. Abee, *Bacillus cereus* ATCC 14579 RpoN (sigma 54) is a pleiotropic regulator of growth, carbohydrate metabolism, motility, biofilm formation and toxin production, PLoS One 10 (2015) e0134872.
[47] P. Bisicchia, E. Lioliou, D. Noone, L.I. Salzberg, et al., Peptidoglycan metabolism is controlled by the WalRK (YycFG) and PhoPR two-component systems in phosphate-limited *Bacillus subtilis* cells, Mol. Microbiol. 75 (2010) 972–989.
[48] O. Kurnasov, L. Jablonski, B. Polanuyer, P. Dorrestein, et al., Aerobic tryptophan degradation pathway in bacteria: novel kynurenine formamidase, FEMS (Fed. Eur. Microbiol. Soc.) Microbiol. Lett. 227 (2003) 219–227.
[49] P. Paul, P. Chakraborty, R.K. Sarker, A. Chatterjee, et al., Tryptophan interferes with the quorum sensing and cell surface hydrophobicity of *Staphylococcus aureus*: a promising approach to inhibit the biofilm development, 3 Biotech 11 (2021) 376.
[50] C. Prasad, V.R. Srinivasan, Tryptophan catabolism during sporulation in B, acillus cereus Biochem J 119 (1970) 343–349.
[51] X.-H. Li, S.-K. Kim, J.-H. Lee, Anti-biofilm effects of anthranilate on a broad range of bacteria, Sci. Rep. 7 (2017) 8604.
[52] U. Olsson, A. Billberg, S. Sjövall, S. Al-Karadaghi, M. Hansson, In vivo and in vitro studies of *Bacillus subtilis* ferrochelatase mutants suggest substrate channeling in the heme biosynthesis pathway, J. Bacteriol. 184 (2002) 4018–4024.
[53] A.I. Celis, J.E. Choby, J. Kentro, E.P. Skaar, J.L. DuBois, Control of metabolite flux during the final steps of heme *b* biosynthesis in gram-positive bacteria, Biochemistry 58 (2019) 5259.
[54] N. Falb, G. Patil, P.G. Furtmüller, T. Gabler, S. Hofbauer, Structural aspects of enzymes involved in prokaryotic Gram-positive heme biosynthesis, Comput. Struct. Biotechnol. J. 21 (2023) 3933–3945.
[55] J. Zamarreño Beas, M.A.M. Videira, L.M. Saraiva, Regulation of bacterial haem biosynthesis, Coord. Chem. Rev. 452 (2022) 214286.
[56] A.A. Yeliseev, S. Kaplan, A novel mechanism for the regulation of photosynthesis gene expression by the TspO outer membrane protein of *Rhodobacter sphaeroides*, J. Biol. Chem. 274 (1999) 21234–21243.
[57] C. Leneveu-Jenvrin, N. Connil, E. Bouffartigues, V. Papadopoulos, et al., Structure-to-function relationships of bacterial translocator protein (TSPO): a focus on *Pseudomonas*, Front. Microbiol. 5 (2014).
[58] J. Liu, C. Hiser, F. Li, R. Hall, et al., New TSPO crystal structures of mutant and heme-bound forms with altered flexibility, ligand binding, and porphyrin degradation activity, Biochemistry 62 (2023) 1262–1273.
[59] D. Guillaumot, S. Guillon, T. Déplanque, C. Vanhee, et al., The *Arabidopsis* TSPO-related protein is a stress and abscisic acid-regulated, endoplasmic reticulum–Golgi-localized membrane protein, Plant J. 60 (2009) 242–256.
[60] C. Vanhee, G. Zapotoczny, D. Masquelier, M. Ghislain, H. Batoko, The *Arabidopsis* multistress regulator TSPO is a heme binding membrane protein and a potential scavenger of porphyrins via an autophagy-dependent degradation mechanism, Plant Cell 23 (2011) 785–805.
[61] A.A.-B. Badawy, Kynurenine pathway of tryptophan metabolism: regulatory and functional aspects, Int. J. Tryptophan Res. 10 (2017) 1178646917691938.
[62] H.J. Yuasa, H.J. Ball, Efficient tryptophan-catabolizing activity is consistently conserved through evolution of TDO enzymes, but not Ido enzymes, J. Exp. Zool. B Mol. Dev. Evol. 324 (2015) 128–140.